ADVANCED MATERIALS
www.advmat.de

Rapid Surface Reconstruction in Air-Processed Perovskite Solar Cells by Blade Coating

Jing Zhuang, Chunki Liu, Bochun Kang, Haiyang Cheng, Mingchao Xiao, Li Li, and Feng Yan**

Blade coating has been developed to be an essential technique for large-area fabrication of perovskite solar cells (PSCs). However, effective surface treatment of the perovskite layer, which is a critical step for improving PSC performance, remains challenges during blade coating due to the short interaction time between the modification solution and the perovskite layer, as well as the limited selection of available organic solvents. In this study, a novel modifier *N*,*N*-diphenylguanidine monohydrobromide (DPGABr) dissolved in acetonitrile (ACN) is blade coated on the $MA_{0.7}FA_{0.3}PbI_3$ surface in air to reconstruct the perovskite surface in hundreds of milliseconds. This work finds that the solvent ACN rapidly dissolves organic iodide of the perovskite layer and leads to a PbI_2-rich surface, providing reactive sites for DPGABr to form a thin DPGABr/PbI_2 complex layer. This surface reconstruction can effectively passivate defects and induce n-type doping on the perovskite surface to facilitate electron transfer. The resultant devices show a 15% improvement in average power conversion efficiency. More importantly, the devices with the surface reconstruction show outstanding long-term stability, with negligible performance degradation even after 1-year storage in air. This study presents a convenient and effective approach for improving the performance of blade-coated PSCs prepared in air.

1. Introduction

In recent years, metal halide perovskite solar cells (PSCs) have gained significant attention in both scientific research and industrial efforts within the photovoltaic community, due to their skyrocketed increase in power conversion efficiency (PCE).[1–5] Blade coating in air stands out as a highly effective and cost-efficient method for producing PSCs on a large scale.[6,7] Moreover, its compatibility with flexible substrates makes it an ideal choice for manufacturing flexible devices.[8,9] At the early stage, researchers were focusing on the operation conditions of blade coating, including substrate temperature,[10] flow speed, and direction of N_2 knife[11] and air humidity.[12] Then more strategies, such as solvent and additives engineering,[13,14] have successfully facilitated the production of high-quality and large-area perovskite films. Notably, in comparison with ordered crystal structure in the bulk, atoms at the perovskite surface are more vulnerable to environment during crystallization. The environmental factors, such as humidity,[15–17] temperature,[18,19] and atmosphere,[20] can influence the crystal lattice and perturb the atomic periodicity on the surface. Therefore, the surface of blade-coated perovskite film, which closely involves charge trapping, carrier recombination, charge transfer, and ion diffusion, plays a crucial role on the performance of resultant PSCs.[21–23]

Many efforts have been devoted to improving the surface quality of perovskite films by surface treatments, such as surface modification or surface reconstruction.[24,25] Typically, surface modification involves the optimization of the chemical or physical properties of perovskite's surface without changing its bulk properties, which is often achieved by introducing small molecule/polymer treatment[26,27] (e.g., Lewis base/acid) or physical modification (such as mechanical peel-off of the defective layer[28]). These processes can enhance the quality of perovskite surfaces with decreased defect density. On the other hand, surface reconstruction is a spontaneous process that typically occurs when introducing molecules on the perovskite surface to react and form a new and more stable structure. The PbI_2 or MAI-terminations of perovskite films serve as a foundation for surface reconstruction at the molecular level, stimulating the physical and chemical alteration of the film surfaces.[29] For example, Wu et al. introduced FAI on the $MAPbI_3$ surface to spontaneously form $FAPbI_3$ through reacting with PbI_2 termination by immersing blade-coated $MAPbI_3$ into

J. Zhuang, C. Liu, B. Kang, H. Cheng, M. Xiao, F. Yan
Department of Applied Physics
The Hong Kong Polytechnic University
Hung Hom, Kowloon, Hong Kong P. R. China
E-mail: apafyan@polyu.edu.hk
L. Li
School of Fashion and Textiles
The Hong Kong Polytechnic University
Hung Hom, Kowloon, Hong Kong P. R. China
E-mail: li.lilly@polyu.edu.hk
F. Yan
Research Institute of Intelligent Wearable Systems
The Hong Kong Polytechnic University
Hung Hom, Kowloon, Hong Kong P. R. China

The ORCID identification number(s) for the author(s) of this article can be found under https://doi.org/10.1002/adma.202309869

DOI: 10.1002/adma.202309869

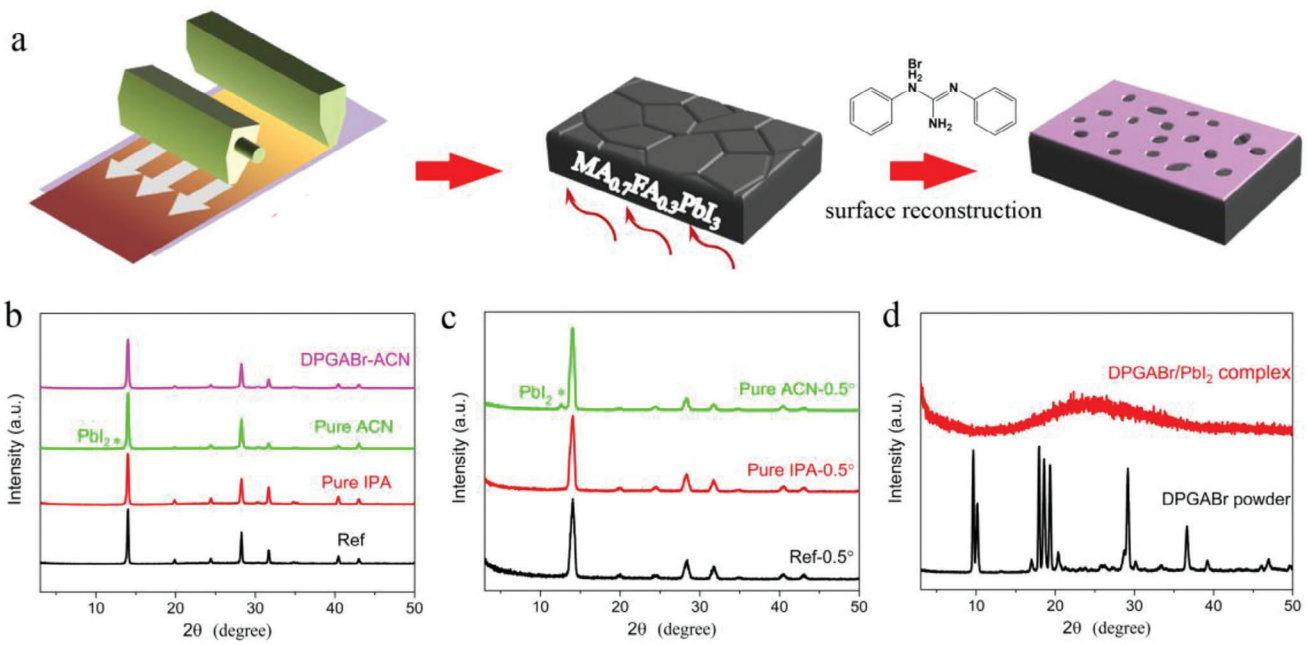

Figure 1. a) Schematic illustration of the surface reconstruction of $MA_{0.7}FA_{0.3}PbI_3$ films by blade coating. b) X-ray diffraction (XRD) patterns of perovskite films with and without posttreatments. c) Grazing incidence XRD (GIXRD) diffraction patterns of the reference perovskite, pure isopropanol (IPA) treated film, and pure acetonitrile (ACN) treated film measured with an incident angle of 0.5°. d) XRD patterns of diphenylguanidine monohydrobromide (DPGABr) powder and DPGABr/PbI_2 complex films.

a hot bath of FAI. This surface reconstruction can effectively reduce surface defect density and promote charge transport at the interface of perovskite and charges transport layers. However, it is challenging to achieve surface reconstruction directly by blade coating because the retention time of a coated solvent is estimated to be only several hundred milliseconds.[6,30] It is expected that the solvents and modifiers for posttreatments by blade coating are critical to the effect of surface reconstruction of perovskite films, which however have been rarely reported until now.

In this study, we examined the impact of solvents such as isopropanol (IPA) and acetonitrile (ACN) for the posttreatment of mixed perovskite $MA_{0.7}FA_{0.3}PbI_3$ on its surface in air by blade coating. We found that ACN can partially remove MAI/FAI and expose PbI_2 termination on the surface within hundreds of milliseconds, whereas IPA has negligible impact on the surface, indicating that ACN is a more suitable solvent for further surface reconstruction. We then introduced a novel surface modifier, *N*,*N*-diphenylguanidine monohydrobromide (DPGABr), to reconstruct the perovskite film surface. Our results reveal that this treatment can substantially enhance the photovoltaic performance due to an effective surface reconstruction on the perovskite layer. We found that an ultrathin complex layer of DPGABr/PbI_2 is formed on the perovskite surface, which significantly reduces nonradiative recombination and facilitates electron transfer due to the modulation of Fermi energy on the surface. Based on this technique, the inverted PSCs prepared by blade coating in air show a champion PCE of 24.04%, with a relative enhancement of 15% in the average PCE in comparison with the control devices. More importantly, the device with the surface reconstruction shows excellent long-term stability and its performance has negligible degradation even after 1-year storage in air at room temperature.

2. Results and Discussion

2.1. Effect of Solvents Blade-Coated on the Surface of $MA_{0.7}FA_{0.3}PbI_3$ Perovskite

The perovskite films with the component of $MA_{0.7}FA_{0.3}PbI_3$ were prepared by blade coating in air and subsequently thermally annealed at 105 °C for 15 min in air (see **Figure 1a**). Then the films were coated with different solvents including ACN and IPA by blade coating because these solvents can only dissolve 3D perovskite slowly on the surface.[31] The resultant films were characterized using X-ray diffraction (XRD). As shown in Figure 1b, the primary peaks of all films can be attributed to the reflection of $MA_{0.7}FA_{0.3}PbI_3$. It is noteworthy that a [001] peak for PbI_2 crystal at 12.5° was observed in the sample treated with ACN solvent by blade coating, indicating that the MAI/FAI on the perovskite surface was initially dissolved in ACN during the rapid dynamic process, with PbI_2 nanocrystals forming on the surface. However, IPA-treated $MA_{0.7}FA_{0.3}PbI_3$ perovskite did not show PbI_2 phase after the blade coating process, which can be attributed to the lower solubility of MAI/FAI in IPA compared to ACN.[31] During the blade coating process, the trace amount of IPA and instantaneous exposure on the perovskite surface makes it difficult to dissolve MAI or FAI. The films were then characterized by grazing incidence XRD (GIXRD). The peak of PbI_2 can only be observed from the pure ACN-treated films at an incident angle of 0.5° (Figure 1c). In addition, the peak intensity ratio of PbI_2 and $MA_{0.7}FA_{0.3}PbI_3$ phases decreases when the incidence angle is

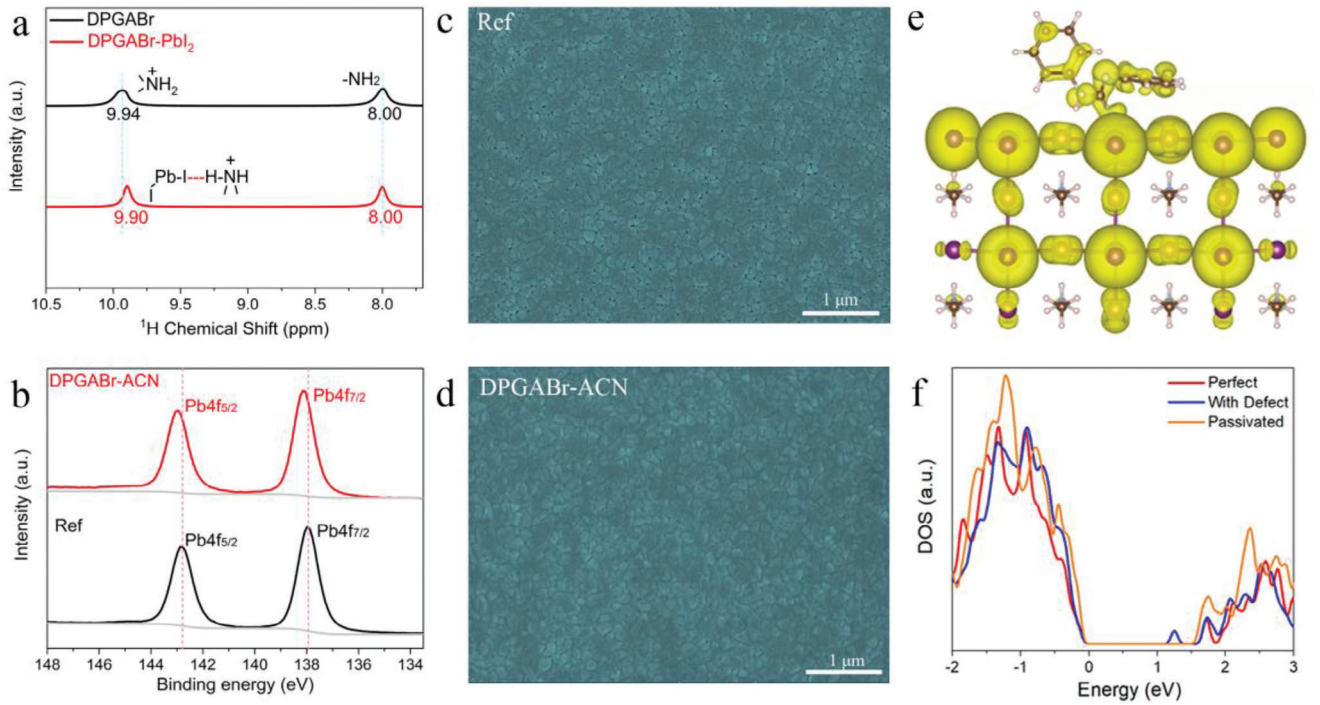

Figure 2. a) ^{1}H-NMR spectra of neat diphenylguanidine monohydrobromide (DPGABr) and DPGABr + PbI_2 compounds. b) X-ray photoelectron spectroscopy (XPS) spectra of Pb4f for reference and DPGABr-ACN treated films. Top-surface scanning electron microscopy (SEM) images of c) reference perovskite films and d) DPGABr-ACN treated film. e) Simulated charge density distribution of $MAPbI_3$ with a Pb_I (I substituted by Pb) antisite defect passivated by DPGABr. f) Density of states (DOS) of perfect $MAPbI_3$, $MAPbI_3$ with a Pb_I antisite defect, and $MAPbI_3$ with a Pb_I antisite defect passivated by DPGABr.

increased to 1° (Figure S1, Supporting Information), indicating that PbI_2 is mainly located on the perovskite surface.

X-ray photoelectron spectroscopy (XPS) spectra of the pristine perovskite film or the films treated with pure ACN or IPA are shown in Figure S2a–c (Supporting Information). The XPS core-level energy spectra of Pb 4f for the pristine perovskite film show two main peaks at 137.95 and 142.83 eV, corresponding to Pb $4f_{7/2}$ and Pb $4f_{5/2}$. In addition, I $3d_{5/2}$ and I$3d_{3/2}$ peak located at 618.9 and 630.3 eV, respectively. The I:Pb ratio can be calculated from the integrated areas of I 3d and Pb 4f peaks. We observed a decline in the I:Pb ratio from 3.15 to 2.68 after the pure ACN post-treatment, confirming the appearance of the PbI_2 termination on the surface. However, the I:Pb ratio of both the pristine film or the IPA-treated films remained unchanged, indicating again that IPA treatment does not have any significant impact on the surface component or chemical characteristics of $MA_{0.7}FA_{0.3}PbI_3$ during the blade coating process.

2.2. Surface Reconstruction of $MA_{0.7}FA_{0.3}PbI_3$ by DPGABr

We selected DPGABr as a surface modifier because its active site $-NH_2^+$ can react with PbI_2 terminations, and meanwhile the $-NH_2$ group can act as a Lewis base to passivate surface defects as reported in previous studies.[27] As presented in Figure 1b, although the perovskite film treated with pure ACN shows the [001] peak for PbI_2, the film blade-coated with the solution of DPGABr dissolved in ACN does not show the PbI_2 [001] peak, indicating that DPGABr can interact with PbI_2 and generate another phase. To study their interaction, mixture of DPGABr and PbI_2 was dissolved in dimethyl formamide (DMF) solvent and deposited on a glass substrate with thermal annealing at 105 °C for 20 min to form a solid film, which was then characterized under XRD. As shown in Figure 1d, the broad peak for the mixture film indicates that DPGABr and PbI_2 can form an amorphous complex while pure DPGABr can crystalize due to the appearance of sharp peaks. Based on our experimental results, we propose a surface reconstruction process wherein the use of ACN as the solvent rapidly dissolves a significant amount of MAI/FAI to expose PbI_2 and then DPGABr interacts with PbI_2 to form a DPGABr/PbI_2 complex.

To gain further insight into the interaction between DPGABr molecules and PbI_2, we conducted nuclear magnetic resonance (NMR) measurement on the solutions of DPGABr or DPGABr + PbI_2 dissolved in d6-DMSO solvent. As shown in **Figure 2a**, the NMR analysis of DPGABr revealed the ^{1}H resonance signals at 9.94 and 8.00 ppm, which correspond to the $-NH_2^+-$ and $-NH_2$ environments of neat DPGABr.[32,33] For the DPGABr + PbI_2 mixture, the ^{1}H resonance signals of $-NH_2^+-$ shifted to 9.90 ppm and that of $-NH_2$ remain unchanged, suggesting the formation of hydrogen bonds between $-NH_2^+-$ and I–Pb–I in the solvent.[34] Then the perovskite films before and after the DPGABr-ACN solution treatment were characterized by XPS. As shown in Figure 2b, the characteristic peaks of Pb 4f in the XPS spectra were found to shift to a higher binding energy from 137.95 to 138.11 eV after the DPGABr-ACN treatment, indicating

the altered chemical environment of Pb and thus the formation of a new phase on the perovskite surface.[35] These results all suggest that DPGABr can interact with PbI_2 induced by ACN coating and generate a thin complex on the perovskite surface.

Scanning electron microscopy (SEM) images of $MA_{0.7}FA_{0.3}PbI_3$ with and without DPGABr-ACN posttreatments are shown in Figure 2c,d. Notably, the perovskite surface treated with DPGABr-ACN exhibited a more compact and smoother morphology compared to the reference film, which is also evidenced by the lower surface roughness observed in atomic force microscopy (AFM) images (Figure S5, Supporting Information). These results indicate that that surface reconstruction was achieved successfully through DPGABr-ACN posttreatment. Energy-dispersive spectroscopy (EDS) mapping of Br elements are shown in Figure S6 (Supporting Information). The sporadic distribution of Br elements suggests that amorphous DPGABr/PbI_2 complex partially cover the perovskite surface, as illustrated in Figure 1a. To explore whether DPGABr can penetrate the perovskite layer, we employed time-of-flight secondary ion mass spectrometry (TOF-SIMS) to detect the vertical distribution of DPGA+ ions. As illustrated in Figure S7 (Supporting Information), the depth profile of DPGA+ decreases rapidly on the surface when the molecular ion ($C_{13}H_{14}N_3$+) is monitored in a positive mode. This observation indicates that DPGABr only permeates to a very shallow depth and is mainly localized on the perovskite surface. This limited penetration can be attributed to the short retention time of DPGABr solution on the perovskite film.

We employed density functional theory (DFT) calculations to investigate the surface properties of films after surface reconstruction. To simplify the calculation while preserving generality, we constructed a cell of the $MAPbI_3$ perovskite with the PbI_2 termination. It is well-known that the band edges of organic–inorganic perovskites are dominated by the orbitals of Pb and I, which are critical to the band structure and closely involve the defects in the cells. Antisite defects related to these ions are known to be located at deep levels of the bandgap, acting as carrier recombination centers that reduce carrier lifetime.[36–38] As a Lewis base, the electron pair of $-NH_2$ in DPGABr enables effective passivation of antisite defects due to the coordination bonding with Pb^{2+},[37] which is also considered as one of the main interactions in our case. Figure S8 (Supporting Information) displays the perovskite supercells with DPGABr passivated defects, providing visual evidence of the coordination bonding between N element in DPGABr and Pb^{2+} at the film surface. To further elucidate the effects of DPGABr passivation, the density of states (DOS) of three conditions, including pristine $MAPbI_3$, $MAPbI_3$ with a Pb_I antisite defect, and $MAPbI_3$ with a Pb_I antisite defect passivated by DPGABr, are simulated and presented in Figure 2e,f. The calculation shows that Pb_I antisite defects induce midgap trap states, but after DPGABr passivation, these trap states are shifted toward the conduction band edge. As such, we conclude that DPGABr can passivate Pb_I antisite defects of perovskite surface and effectively reduce the number of carrier nonradiative recombination centers.

We conducted photoluminescence (PL) measurements on perovskite films with and without surface reconstruction to further evaluate the passivation effects. The tests were performed on perovskite films coated on glass substrates and excited from the perovskite side with 435 nm excitation. **Figure 3a** shows that both films emit infrared light within a wavelength range of approximately 750 to 840 nm, indicating that the incorporation of DPGABr into the perovskite film surface has little impact on the radiative recombination mechanism. However, the DPGABr-ACN treated perovskite film exhibited a stronger PL intensity, suggesting a reduction in nonradiative recombination centers on the surface. This inference is supported by the time-resolved PL (TRPL) results shown in Figure 3b. We fitted the data with a biexponential decay function and calculated the average lifetime τ_{ave} using the following equation[39]:

$$\tau_{ave} = \frac{\sum A_i \tau_i^2}{\sum A_i \tau_i} \quad (1)$$

The resulting τ_{ave} for the reference perovskite films and DPGABr-ACN film was found to be 452 and 791 ns, respectively. The increased τ_{ave} indicates a reduction in nonradiative recombination centers on the perovskite surface after surface reconstructions, which is favorable for improving the photovoltaic performance of PSCs.

To estimate trap densities in the perovskite films, we conducted space charge-limited current (SCLC) tests, and the inset of Figure 3c shows the electron-only device with a structure of ITO/SnO_2/perovskite/$PC_{70}BM$/Ag. Figure 3c demonstrates a trap-filled limit voltage (V_{TFL}) of 0.28 V for the reference device and a lower V_{TFL} of 0.11 V for the DPGABr-ACN treated device. The trap density (N_t) was calculated using the equation[40]:

$$N_t = \frac{2V_{TFL}\varepsilon_r\varepsilon_0}{qL^2} \quad (2)$$

where L represents the thickness of the perovskite film, ϵ_r represents the relative dielectric constant of the perovskite, ϵ_0 represents the vacuum permittivity, and q represents the electron charge. The trap densities for the perovskites before and after DPGABr-ACN treatment are estimated to be 2.05×10^{15} and 8×10^{14} cm^{-3}, respectively. The tests on hole-only devices presented in Figure S9 (Supporting Information) show a similar result, with a reduction in N_t after DPGABr-ACN treatment from 1.32×10^{15} to 9.5×10^{14} cm^{-3}. The decrease in trap density observed in the DPGABr-ACN treated film highlights the potential of surface reconstruction in achieving a high-quality film surface, which is essential for improving V_{oc} in PSCs.

According to the light absorption spectrum of the DPGABr/PbI_2 complex layer, the absorption edge is about 432 nm (Figure S10, Supporting Information), corresponding to the bandgap energy of 3.12 eV, indicating that the complex layer is almost an insulator. The coverage of the insulating complex partially on the perovskite surface can passivate surface traps while charge transfer will not be influenced if it is thin enough. Indeed, the decreased contact area between the electron transport layer and the perovskite layer in a PSC may mitigate carrier recombination in resultant PSCs, which is similar to the previous reports on the effect of an ultrathin poly(methyl methacrylate) (PMMA) interlayer in improving the performance of PSCs.[41,42]

To develop a deeper understanding of charge transfer after surface treatment, we analyzed the energy level alignment of the

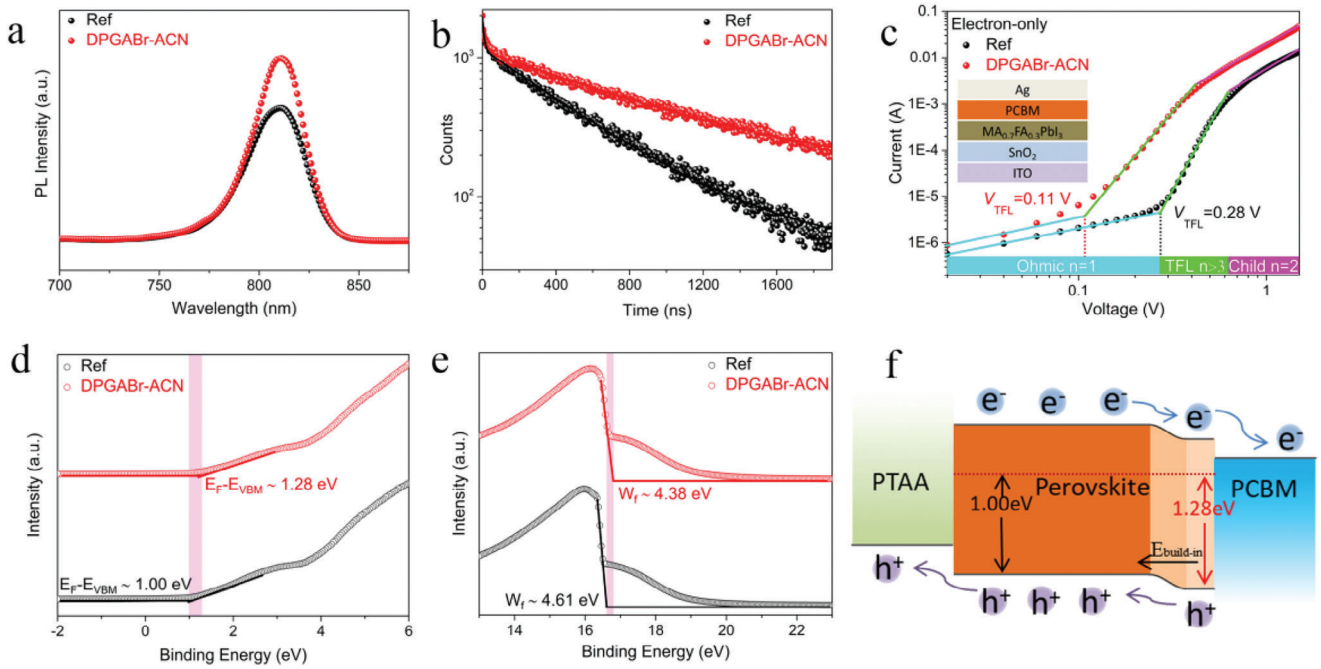

Figure 3. a) Steady-state photoluminescence (PL) and b) time-resolved PL (TRPL) spectra of perovskite films with and without DPGABr-ACN treatment. c) Current–voltage curves for two electron-only devices with the structure of ITO/SnO_2/$MA_{0.7}FA_{0.3}PbI_3$/$PC_{70}BM$/Ag. The two devices correspond to the perovskite films with and without surface reconstruction by DPGABr-ACN. d,e) Ultraviolet photoelectron spectroscopy (UPS) spectra of perovskites with and without DPGABr-ACN treatment. f) Energy level alignment of $MA_{0.7}FA_{0.3}PbI_3$ perovskite solar cells (PSCs) with the DPGABr-ACN treatment.

perovskite films by conducting ultraviolet photoelectron spectroscopy (UPS). Figure 3d,e presents the values of $E_f - E_{VBM}$ and work functions (W_f), respectively, which were extracted from the cutoff of the linear extension line. Our results indicate that the gap between E_f and E_{VBM} becomes wider after the surface treatment, suggesting that the surface of the film is more n-type and that the number of free electrons at the surface increases due to the contribution of Lewis base on the surface.[43] The decrease of W_f from 4.61 to 4.38 eV at the surface results in a reinforced built-in electric field with a direction from the surface to the bulk, which can promote the separation of photogenerated carriers.[43–45] According to the values of $E_f - E_{VBM}$, W_f, and band gap (E_g) extracted from Tauc plots (Figure S12, Supporting Information), the positions of the valence band (E_v) and conduction band (E_c) can be determined. The energy level alignment of the device is shown in Figure 3f, from which the charge transfer characteristic can be analyzed. At a steady state, the Fermi levels in the bulk and on the surface of the perovskite layer should be aligned, resulting in band bending at the bulk/surface junction. This downward band bending enables efficient holes transfer toward the PTAA layer and promotes electron diffusion toward the PCBM layer, which can effectively suppress carrier recombination.

In order to further demonstrate the complete capabilities of surface reconstruction in scalable fabrication of uniform perovskite films, we fabricated 5 × 5 cm perovskite films with surface reconstruction and performed AFM characterizations on different regions. As shown in Figure S13 (Supporting Information), the morphology of the perovskite film is similar in seven regions with little variations in surface roughness, which indicates a uniform morphology of the whole large-area perovskite film. In addition, the UV–Visible absorption spectra of different regions of the perovskite film almost overlap (Figure S14, Supporting Information), demonstrating that the thickness of the whole large-area perovskite film is uniform. Urbach energy (E_u), which quantifies energetic disorder in the band edges of a semiconductor, can be used to assess the quality of the perovskite film in different regions. According to equation[46]:

$$\ln\alpha = \ln\alpha_0 + \frac{1240}{\lambda}\frac{1}{E_u} \quad (3)$$

where α is the absorption coefficientα, α_0 is constant, λ is wavelength, and E_u is Urbach energy. The slope of the data in near-band-edge region (1.53–1.59 V) is associated with E_u of a film. The calculated Urbach energies of the seven different areas of the perovskite film are distributed in a very narrow region of 24.2 ± 0.2 meV (Table S4, Supporting Information). These results fully demonstrate that surface reconstruction is suitable for the fabrication of uniform large-area perovskite films.

2.3. Photovoltaic Properties of DPGABr-Treated PSCs

To explore the effect of different posttreatments on photovoltaic performance, we fabricated PSCs with a structure of ITO/PTAA/$MA_{0.7}FA_{0.3}PbI_3$/$PC_{70}BM$/BCP/Ag (**Figure 4a**) modified with DPGABr-IPA and DPGABr-ACN, respectively. The results in Figure 4b show that DPGABr-IPA treatment had a negligible impact on the PCE of PSCs. However, as shown in

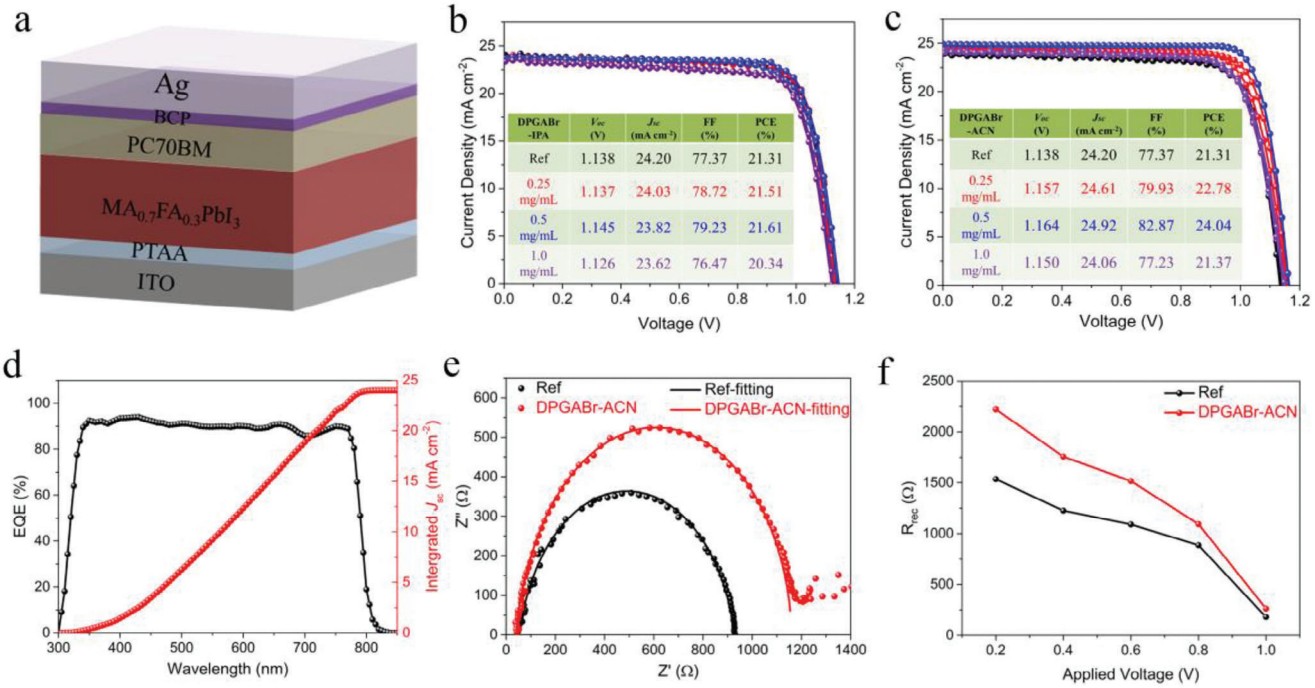

Figure 4. a) Device structure of perovskite solar cell (PSC). *J–V* curves of PSCs with different concentrations of b) DPGABr-IPA treatment and c) DPGABr-ACN treatment. Insets: photovoltaic performance parameters. d) External quantum efficiency (EQE) spectra of the PSC with 0.5 mg mL^{-1} DPGABr-ACN treatment. e) Electrochemical impedance spectroscopy (EIS) of $MA_{0.7}FA_{0.3}PbI_3$ PSCs measured at a bias voltage of 0.80 V under light illumination of 100 mW cm^{-2}. f) The R_{rec} of the $MA_{0.7}FA_{0.3}PbI_3$ PSCs derived from EIS at various voltages under light illumination of 100 mW cm^{-2}.

Figure 4c, DPGABr-ACN treatment significantly improved the PCE from 21.31% to 24.04%, along with an enhanced V_{oc} of 1.164 V, short-circuit current (J_{sc}) of 24.92 mA cm^{-2}, and fill factor (FF) of 82.87%. In addition, external quantum efficiency (EQE) measurements (Figure 4d) show that the integrated photocurrent of the champion device is 24.01 mA cm^{-2}, which is consistent with the J_{sc} value obtained from the *J–V* curves. These results suggest that surface reconstruction by DPGABr-ACN treatment can enhance the photovoltaic performance of PSCs. To demonstrate that the difference in photovoltaic performance is caused by surface reconstruction rather than pure solvent effects, we fabricated the PSCs modified with two different pure solvents. As shown in Figure S16 (Supporting Information), surface treatment with pure solvent can hardly improve the photovoltaic performance of the devices.

To gain further insight into the underlying mechanisms of charge transport and recombination in the PSCs, we characterized the devices with electrochemical impedance spectroscopy (EIS). Figure 4e shows the Nyquist plots measured at a bias voltage of 0.80 V under light illumination of 100 mW cm^{-2}. The equivalent circuit model shown in Figure S17c (Supporting Information) was used to obtain the charge transfer resistance (R_{tr}) and recombination resistance (R_{rec}). Generally, the high-frequency component represents R_{tr}, while the low-frequency component represents R_{rec}.[47] Specifically, we observed a decrease in R_{tr} from 55.38 to 26.68 Ω, as well as an increase in R_{rec} from 885.4 to 1094 Ω for devices before and after the DPGABr-ACN treatment. These findings suggest that surface reconstruction led to faster charge transport and reduced nonradiative recombination at the perovskite/PCBM interface, which is beneficial for J_{sc} and V_{oc} of PSCs. In Figure 4f, we present R_{rec} values at various applied voltages under light illumination of 100 mW cm^{-2}. It can be observed that the target device shows higher R_{rec} than that of the control device at every bias voltage. This finding provides strong evidence that surface reconstruction can significantly reduce recombination rate in the PSCs due to the defect passivation by DPGABr.

Figure 5a shows the dependence of V_{oc} on light intensity in PSCs with and without DPGABr-ACN treatment. This analysis can offer more comprehensive insights into the recombination process occurring under open-circuit conditions. According to the equation:[48]

$$\delta \mathrm{Voc} = \frac{nK_B T}{q} \ln(I) + \text{constant} \quad (4)$$

where n is the ideality factor, K_B is the Boltzmann constant, q is the elementary charge, T is the absolute temperature, and I is the light intensity. The V_{oc} varies linearly with the logarithm of I. The corresponding slopes, nK_BT/q, for the target and control devices were determined to be 1.36 K_BT/q and 1.51 K_BT/q, respectively. Generally, a larger deviation from the ideal slope of 1 KT/q suggests the presence of more trap-assisted recombination centers.[49] The lower slope observed in the DPGABr-ACN treated PSC indicates that nonradiative recombination was effectively suppressed. In addition, dark *I–V* curve measurements were carried out to examine the reverse saturation current density of PSCs. As shown in Figure 5b, the target PSC exhibits a

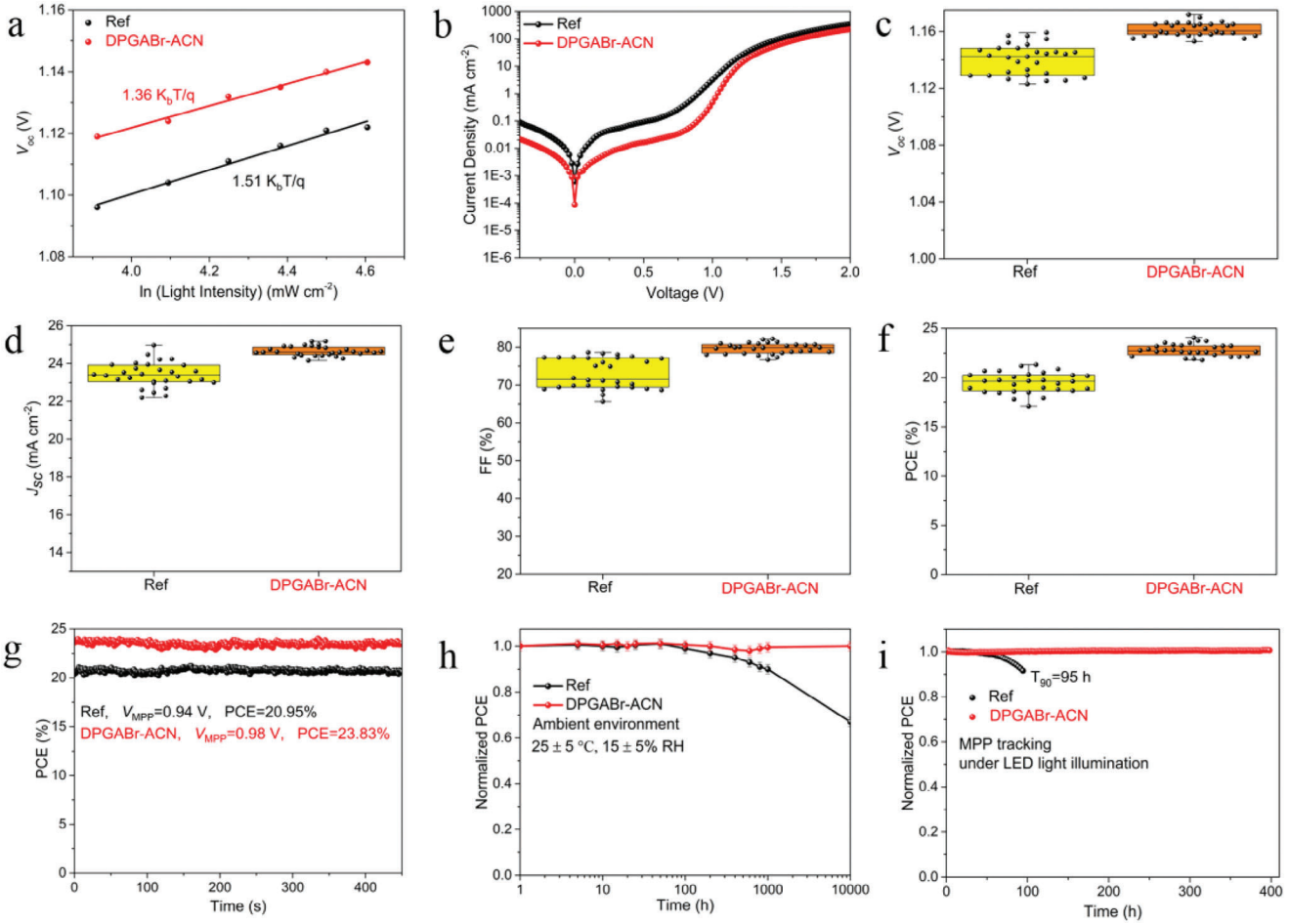

Figure 5. a) V_{oc} as a function of light intensity for the perovskite solar cells (PSCs) with and without DPGABr-ACN treatment. b) Dark *J*--*V* curves of the PSCs with and without DPGABr-ACN treatment. The statistics of performance parameters for devices with and without DPGABr-ACN: c) V_{oc}, d) J_{sc}, e) fill factor (FF), and f) power conversion efficiency (PCE). g) Stabilized power output of PSCs tracked at the maximum power point (MPP) under AM 1.5G illumination. h) Long-term storage stability of the PSCs in ambient air. i) Long-term operational stability of the encapsulated PSCs tracked at the MPP under light emitting diode (LED) light illumination with an intensity of 100 mW cm^{-2} in ambient air.

lower reverse saturation current density than the control device, indicating that carrier generation rate in the dark is lower in the former due to lower trap density.[50] This result is consistent with the suppressed recombination rate in the target PSCs.

To assess the repeatability of DPGABr-ACN treatment, we fabricated 30 devices in the same batch to evaluate the performance enhancement. Figure 5c–f and Table S7 (Supporting Information) shows that DPGABr-ACN-treated devices outperform the reference devices in terms of average V_{oc}, J_{sc}, FF, and PCE. We also evaluated the stabilized power output of PSCs at the maximum power point (MPP) under AM 1.5G illumination. In Figure 5g, the results indicate that the PSC treated with DPGABr-ACN exhibits a higher output PCE of 23.83% at the V_{MPP} of 0.98 V, compared to the control device with a PCE of 20.95% at the applied voltage of 0.94 V. Notably, both devices maintained a stable output during operation. In addition, long-term stability of PSCs is crucial to practical applications. Figure 5h depicts the long-term storage stability of the PSCs under ambient conditions (25 ± 5 °C, 15% ± 5% RH). The target device exhibits excellent stability in 10 000 h (≈400 days) while the control device shows obvious degradation in the same period, which can be attributed to the coverage of a thin DPGABr/PbI_2 complex layer on the perovskite surface. We further monitored the operational stability of PSCs at MPP in air ambient (25 ± 5 °C, 15% ± 5% RH) (Figure 5i). The encapsulated PSC treated with DPGABr-ACN retained its original PCE after 400 h of white light illumination with an intensity of 100 mW cm^{-2} from a light emitting diode (LED). In comparison, the PCE of reference device decreased to 90% of its initial efficiency after 95 h. Moreover, compared to previously reported blade-coated devices (Table S8, Supporting information), our devices exhibit superior long-term stability, suggesting that the unique technique of surface reconstruction opens up promising avenues for the practical applications of PSCs in the near future.

3. Conclusion

In summary, we present a facile blade-coating approach to reconstructing a perovskite surface with the DPGABr-CAN solution, which is very effective on improving the performance of

air-processed blade-coated PSCs. ACN can dissolve and remove MAI/FAI quickly on the perovskite surface, leading to the exposure of PbI_2, and DPGABr can enable surface reconstruction through the reaction with PbI_2 termination, yielding a thin amorphous complex that covers the perovskite surface. We found that the DPGABr/PbI_2 complex layer can passivate defects and tune the perovskite surface to be more n-type. Consequently, the devices after the treatment show higher PCE with a relative enhancement of 15% and a superior air storage stability in 10000 h. This work provides a novel strategy for surface reconstruction of perovskite films by blade-coating, which is compatible with upscaling manufacture of large-area perovskite films and other optoelectronic perovskite devices.

Supporting Information

Supporting Information is available from the Wiley Online Library or from the author.

Acknowledgements

This work was supported by the Research Grants Council of Hong Kong, China (Project No. 15306822), the Hong Kong Polytechnic University, Hong Kong, China (ZE2X). This work was also supported by Shenzhen Science and Technology Innovation Commission (Project No. SGDX20210823103401011). L.L. thanks the supports by the NSFC General Program (Grant Number 32071906) from National Natural Science Foundation of China.

Conflict of Interest

The authors declare no conflict of interest.

Data Availability Statement

The data that support the findings of this study are available from the corresponding author upon reasonable request.

Keywords

air processed, blade coating, perovskite solar cells, surface reconstruction

Received: September 22, 2023
Revised: November 18, 2023
Published online: December 6, 2023

[1] A. Kojima, K. Teshima, Y. Shirai, T. Miyasaka, *J. Am. Chem. Soc.* **2009**, *131*, 6050.
[2] A. Mei, X. Li, L. Liu, Z. Ku, T. Liu, Y. Rong, M. Xu, M. Hu, J. Chen, Y. Yang, M. Grätzel, H. Han, *Science* **2014**, *345*, 295.
[3] Z. Xiao, Q. Dong, C. Bi, Y. Shao, Y. Yuan, J. Huang, *Adv. Mater.* **2014**, *26*, 6503.
[4] J. H. Heo, D. H. Song, H. J.i Han, S. Y. Kim, J. H. Kim, D. Kim, H. W. Shin, T. K. Ahn, C. Wolf, T.-W. Lee, S. H. Im, *Adv. Mater.* **2015**, *27*, 3424.
[5] N. J. Jeon, J. H. Noh, W. S. Yang, Y. C. Kim, S. Ryu, J. Seo, S. I. l. Seok, *Nature* **2015**, *517*, 476.
[6] Y. Deng, E. Peng, Y. Shao, Z. Xiao, Q. Dong, J. Huang, *Energy Environ. Sci.* **2015**, *8*, 1544.
[7] Y. Deng, Q. Dong, C. Bi, Y. Yuan, J. Huang, *Adv. Energy Mater.* **2016**, *6*, 1600372.
[8] J. Nie, Y. Zhang, L. Li, Y. Zhang, *Adv. Devices Instrum.* **2023**, *4*, 0025.
[9] Y. Dong, J. Ma, S. Yang, H. Yang, *Adv. Devices Instrum.* **2023**, *4*, 0011.
[10] Y. Zhong, R. Munir, J. Li, M.-C. Tang, M. R. Niazi, D.-M. Smilgies, K. Zhao, A. Amassian, *ACS Energy Lett.* **2018**, *3*, 1078.
[11] P. W.-K. Fong, H. Hu, Z. Ren, K. Liu, L. Cui, T. Bi, Q. Liang, Z. Wu, J. Hao, G. Li, *Adv. Sci.* **2021**, *8*, 2003359.
[12] J. Hidalgo, C. A. R. Perini, A.-F. Castro-Mendez, D. Jones, H. Köbler, B. Lai, R. Li, S. Sun, A. Abate, J.-P. Correa-Baena, *ACS Energy Lett.* **2020**, *5*, 3526.
[13] S. Chen, X. Dai, S. Xu, H. Jiao, L. Zhao, J. Huang, *Science* **2021**, *373*, 902.
[14] S. Chen, X. Xiao, H. Gu, J. Huang, *Sci. Adv.* **2021**, *7*, eabe8130.
[15] G. Wang, Q. Lian, D. Wang, F. Jiang, G. Mi, D. Li, Y. Huang, Y. Wang, X. Yao, R. Shi, C. Liao, J. Zheng, A. Ho-Baillie, A. Amini, B. Xu, C. Cheng, *Adv. Mater.* **2022**, *34*, 2205143.
[16] P. W.-K. Fong, H. Hu, Z. Ren, K. Liu, L. Cui, T. Bi, Q. Liang, Z. Wu, J. Hao, G. Li, *Adv. Sci.* **2021**, *8*, 2003359.
[17] H. Li, X. Feng, K. Huang, S. Lu, X. Wang, E. Feng, J. Chang, C. Long, Y. Gao, Z. Chen, C. Yi, J. He, J. Yang, *Small* **2023**, *19*, 2300374.
[18] Y. Chen, X. Liu, Y. Zhao, *Angew. Chem., Int. Ed.* **2022**, *61*, 202110603.
[19] J. A. Aguiar, S. Wozny, N. R. Alkurd, M. Yang, L. Kovarik, T. G. Holesinger, M. Al-Jassim, K. Zhu, W. Zhou, J. J. Berry, *ACS Energy Lett.* **2016**, *1*, 155.
[20] S. Pathak, A. Sepe, A. Sadhanala, F. Deschler, A. Haghighirad, N. Sakai, K. C. Goedel, S. D. Stranks, N. Noel, M. Price, S. Hüttner, N. A. Hawkins, R. H. Friend, U. Steiner, H. J. Snaith, *ACS Nano* **2015**, *9*, 2311.
[21] Q. Jiang, Y. Zhao, X. Zhang, X. Yang, Y. Chen, Z. Chu, Q. Ye, X. Li, Z. Yin, J. You, *Nat. Photonics* **2019**, *13*, 460.
[22] D. Luo, X. Li, A. Dumont, H. Yu, Z.-H. Lu, *Adv. Mater.* **2021**, *33*, 2006004.
[23] G. Wu, R. Liang, M. Ge, G. Sun, Y. Zhang, G. Xing, *Adv. Mater.* **2022**, *34*, 2105635.
[24] Q. Jiang, J. Tong, Y. Xian, R. A. Kerner, S. P. Dunfield, C. Xiao, R. A. Scheidt, D. Kuciauskas, X. Wang, M. P. Hautzinger, R. Tirawat, M. C. Beard, D. P. Fenning, J. J. Berry, B. W. Larson, Y. Yan, K. Zhu, *Nature* **2022**, *611*, 278.
[25] Z. Li, B. Li, X. Wu, S. A. Sheppard, S. Zhang, D. Gao, N. J. Long, Z. Zhu, *Science* **2022**, *376*, 416.
[26] M. Yang, T. Zhang, P. Schulz, Z. Li, G. Li, D. H. Kim, N. Guo, J. J. Berry, K. Zhu, Y. Zhao, *Nat. Commun.* **2016**, *7*, 12305.
[27] F. Li, X. Deng, F. Qi, Z. Li, D. Liu, D. Shen, M. Qin, S. Wu, F. Lin, S.-H. Jang, J. Zhang, X. Lu, D. Lei, C.-S. Lee, Z. Zhu, A. K.-Y. Jen, *J. Am. Chem. Soc.* **2020**, *142*, 20134.
[28] S. Chen, Y. Liu, X. Xiao, Z. Yu, Y. Deng, X. Dai, Z. Ni, J. Huang, *Joule* **2020**, *4*, 2661.
[29] Y. Yang, W. Zhao, T. Yang, J. Liu, J. Zhang, Y. Fang, S. F. Liu, *J. Mater. Chem. A* **2021**, *9*, 23597.
[30] Y. Deng, C. H. Van Brackle, X. Dai, J. Zhao, B. Chen, J. Huang, *Sci. Adv.* **2019**, *5*, eaax7537.
[31] S. Sidhik, Y. Wang, M. De Siena, R. Asadpour, A. J. Torma, T. Terlier, K. Ho, W. Li, A. B. Puthirath, X. Shuai, A. Agrawal, B. Traore, M. Jones, R. Giridharagopal, P. M. Ajayan, J. Strzalka, D. S. Ginger, C. Katan, M. A. Alam, J. Even, M. G. Kanatzidis, A. D. Mohite, *Science* **2022**, *377*, 1425.
[32] J. Zhu, S. Park, O. Y. Gong, C. Sohn, Z. Li, Z. Zhang, B. Jo, W. Kim, G. S. Han, D. H. Kim, T. K. Ahn, J. Lee, H. S. Jung, *Energy Environ. Sci.* **2021**, *14*, 4903.

[33] X. Li, M. Ibrahim Dar, C. Yi, J. Luo, M. Tschumi, S. M. Zakeeruddin, M. K. Nazeeruddin, H. Han, M. Grätzel, *Nat. Chem.* **2015**, *7*, 703.
[34] T. Yang, L. Gao, J. Lu, C. Ma, Y. Du, P. Wang, Z. Ding, S. Wang, P. Xu, D. Liu, H. Li, X. Chang, J. Fang, W. Tian, Y. Yang, S. Liu, K. Zhao, *Nat. Commun.* **2023**, *14*, 839.
[35] S. Tan, T. Huang, I. Yavuz, R. Wang, M. H. Weber, Y. Zhao, M. Abdelsamie, M. E. Liao, H.-C. Wang, K. Huynh, K.-H. Wei, J. Xue, F. Babbe, M. S. Goorsky, J.-W. Lee, C. M. Sutter-Fella, Y. Yang, *J. Am. Chem. Soc.* **2021**, *143*, 6781.
[36] H. Cheng, C. Liu, J. Zhuang, J. Cao, T. Wang, W.-Y. Wong, F. Yan, *Adv. Funct. Mater.* **2022**, *32*, 2204880.
[37] R. Yu, G. Wu, R. Shi, Z. Ma, Q. Dang, Y. Qing, C. Zhang, K. Xu, Z. Tan, *Adv. Energy Mater.* **2023**, *13*, 2203127.
[38] J. Cao, C.-K. Liu, V. Piradi, H.-L. Loi, T. Wang, H. Cheng, X. Zhu, F. Yan, *ACS Energy Lett.* **2022**, *7*, 3362.
[39] J. Zhuang, P. Mao, Y. Luan, N. Chen, X. Cao, G. Niu, F. Jia, F. Wang, S. Cao, J. Wang, *Adv. Funct. Mater.* **2021**, *31*, 2010385.
[40] J. Cao, H.-L. Loi, Y. Xu, X. Guo, N. Wang, C.-K. Liu, T. Wang, H. Cheng, Y. Zhu, M. G. Li, W.-Y. Wong, F. Yan, *Adv. Mater.* **2022**, *34*, 2107729.
[41] H. Kim, K. S. Lee, M. J. Paik, D. Y. Lee, S.-U. Lee, E. Choi, J. S. Yun, S. I. l. Seok, *Adv. Funct. Mater.* **2022**, *32*, 2110473.
[42] B. Yuan, C. Li, W. Yi, F. Juan, H. Yu, F. Xu, C. Li, B. Cao, *J. Phys. Chem. Solids* **2021**, *153*, 110000.
[43] Y.-N. Lu, J.-X. Zhong, Y. Yu, X. Chen, C.-Y. Yao, C. Zhang, M. Yang, W. Feng, Y. Jiang, Y. Tan, L. Gong, X. Wei, Y. Zhou, L. Wang, W.-Q. Wu, *Energy Environ. Sci.* **2021**, *14*, 4048.
[44] W. Yan, Y. Li, Y. Li, S. Ye, Z. Liu, S. Wang, Z. Bian, C. Huang, *Nano Energy* **2015**, *16*, 428.
[45] W. Chai, W. Zhu, Z. Zhang, D. Liu, Y. Ni, Z. Song, P. Dong, D. Chen, J. Zhang, C. Zhang, Y. Hao, *Chem. Eng. J.* **2023**, *452*, 139292.
[46] Y. Gao, Y. Wu, H. Lu, C. Chen, Y. Liu, X. Bai, L. Yang, W. W. Yu, Q. Dai, Y. Zhang, *Nano Energy* **2019**, *59*, 517.
[47] H. Li, J. Cao, Q. Zhou, L. Ding, J. Wang, *Nano Energy* **2015**, *15*, 125.
[48] C. Chen, D. Liu, B. Zhang, W. Bi, H. Li, J. Jin, X. Chen, L. Xu, H. Song, Q. Dai, *Adv. Energy Mater.* **2018**, *8*, 1703659.
[49] M. Du, S. Zhao, L. Duan, Y. Cao, H. Wang, Y. Sun, L. Wang, X. Zhu, J. Feng, L. Liu, X. Jiang, Q. Dong, Y. Shi, K. Wang, S. Liu, *Joule* **2022**, *6*, 1931.
[50] T. Wu, P. Xu, D. Wang, X. Jiang, F. Guo, S. Gao, Z. Ge, Y. Zhang, *Chem. Eng. J.* **2023**, *454*, 140451.